Bennouk, A.; Nejmi, A.; Ramzi, M.

Article

Stability enhancement of a wind plant based on a DFIG and a PMSM: A Lyapunov approach

Energy Reports

Provided in Cooperation with:
Elsevier

Suggested Citation: Bennouk, A.; Nejmi, A.; Ramzi, M. (2018) : Stability enhancement of a wind plant based on a DFIG and a PMSM: A Lyapunov approach, Energy Reports, ISSN 2352-4847, Elsevier, Amsterdam, Vol. 4, pp. 13-22, https://doi.org/10.1016/j.egyr.2017.10.001

Energy Reports 4 (2018) 13–22

Contents lists available at ScienceDirect

Energy Reports

journal homepage: www.elsevier.com/locate/egyr

Stability enhancement of a wind plant based on a DFIG and a PMSM: A Lyapunov approach

A. Bennouk *, A. Nejmi, M. Ramzi

Laboratory of Mathematics and physics, Faculty of Sciences and Technics, Sultan Moulay Slimane University, Beni Mellal, Morocco

ARTICLE INFO

Article history:
Received 10 May 2017
Received in revised form 15 September 2017
Accepted 4 October 2017

Keywords:
Wind turbine
PMSM
DFIG
MSC
GSC
MPPT
Lyapunov
Transmission grid

ABSTRACT

This paper presents a hybrid wind generation with a doubly-fed induction generator (DFIG) and a permanent magnet synchronous machine (PMSM). The study analyzes the performances of the two wind systems and assets the stability of the operating parameters in the presence of a grid fault. Both the DFIG and PMSM Machine-Side Converter (MSC) nonlinear commands are built according to Lyapunov conditions, while the Grid-Side Converter (GSC) command is based on a standard vector control. In the first stage, the control of a 1.5 MW DFIG is presented. Then, the hybrid system including the two wind turbines is presented. Stability performances analysis is based on the verification of the standard operating parameters. The simulation is carried under Matlab/Simulink.

1. Introduction

Wind energy is currently one of the backbones of renewable energy production. This is made possible by the advancement in offshore and onshore wind technologies, in addition to the fact that the price of produced MWH by wind turbines is becoming more and more competitive.

Among the most widespread wind driven generators, the Permanent Magnet Synchronous Machine (PMSM) offers several advantages. Mainly, the direct drive without multiplier reduces maintenance costs. But, the cost of full-scale converters, which must have the same power as the generator, makes the cost of this system less competitive, in comparison to the DFIG wind turbine. A DFIG wind turbine generally requires a Gearbox to adapt the turbine speed to the speed of the generator, this fact increases the maintenance cost. But the converters are more competitive, since they are partially loaded, being dimensioned according to the rotor power (Rajendran and Jena, 2015).

The main purpose of the study is to examine the possibility of connecting two different wind turbines in a common grid, by assessing the global stability and system performances, before any real connection in a physical plant. The control strategy is based upon Lyapunov functions to assure the system's stability in the presence of wind fluctuations and grid fault. In addition, a similar real case is presented to validate results carried out by simulation.

We first present a large scale DFIG wind driven turbine (1.5 MW) control strategy, and explain the MSC and GSC commands. Then, we present a hybrid system based on wind driven DFIG and PMSM, connected to the main grid. The command strategy is based on the flux oriented control according to the Lyapunov conditions, in presence of wind speed fluctuations. The study permits the assessment of the control strategy robustness.

The stability issue is examined according to the energy quality parameters, namely the voltage balance, the harmonic distortion rate (HDR) and the frequency stability at Point of Common Coupling (PCC).

Finally, the results of a real grid fault at the wind plant level are presented. Currents, voltage profiles, HDR, flicker and frequency are examined in order to validate the case study under Matlab/Simulink.

2. Modeling and simulation of a DFIG wind turbine

2.1. Wind speed model

The wind speed model is given by the following equation:

$$\dot{x}(t) = f\left(x\left(t\right), t, u\left(t\right)\right) + w(t). \quad (1)$$

* Corresponding author.
E-mail addresses: bennoukanasse@yahoo.com (A. Bennouk), alinejmi@yahoo.fr (A. Nejmi).

https://doi.org/10.1016/j.egyr.2017.10.001

The measured variables are:

$$y(t) = h(x(t), u(t), t) + e(t). \tag{2}$$

The function f is non-linear, w is a zero mean Gaussian noise with a spectral density $R1(t)$ and $e(t)$, the error, has a spectral density $R2(t)$ (Welch and Bish, 0000).

Wind speed and Gaussian noise are given by:

$$\begin{bmatrix} \dot{v}' \\ \ddot{v}' \end{bmatrix} = \begin{bmatrix} 0 & 1 \\ -\dfrac{1}{p1*p2} & \dfrac{p1+p2}{p1*p2} \end{bmatrix} \begin{bmatrix} v' \\ \dot{v}' \end{bmatrix} + \begin{bmatrix} 0 \\ \dfrac{k}{p1*p2} \end{bmatrix} ev \tag{3}$$

$$v' = \begin{bmatrix} 1 & 0 \end{bmatrix} \begin{bmatrix} v' \\ \dot{v}' \end{bmatrix}$$

v' is the fictitious wind speed, which would be used to estimate the wind speed. The values of p_1 and p_2 are given in order to have a good estimate and to reduce the difference with the actual speed (Welch and Bish, 0000).

2.2. Power coefficient and MPPT strategy

In this section, we define a means to allow the turbine to operate under normal conditions, while regulating the mechanical angular velocity to damp and absorb fluctuations, in response to high wind speed instability. In fact the power coefficient (Cp) must be maintained at a maximum, which suppose a specific velocity and a well-defined beta angle of the blades. The angle beta (β) is exploited especially at high speed in order to limit the vibrations at the level of the blades (Lee et al., 2011, 2012):

$$Cp = C_1 \left(\frac{C_2}{\lambda i} - C_3\beta - C_4\beta^6 \right) e^{-\frac{C5}{\lambda i}} - C_6\lambda. \tag{4}$$

Assuming that β is constant and equal to 0 for small wind speed less than 12 m/s, C_i are constant given by turbine manufacturer, the C_p derivative depends on λ_i equal to λ (tip-speed ratio):

$$\frac{dCp}{d\lambda} = -C_1 \left(\frac{C_2}{\lambda^2} \right) e^{-\frac{C5}{\lambda}} + C_1C_5 \left(\frac{C_2}{\lambda^3} \right) e^{-\frac{C5}{\lambda}} - C_6 = 0.$$

Hence, the optimal value of λ is deduced:

$$\lambda_{opt} = \sqrt[3]{\frac{C1.C2.C5 - C1.C2}{C6}}. \tag{5}$$

Substituting the new value of λ in the power coefficient equation, we find the value of C_p corresponding to the optimal power, C_i are constants given by turbine manufacturer.

As long as the wind speed is less than the nominal speed, fixed at 12 m/s (for a 1.5 MW or 2 MW turbine of our study), the reference of the angle β is zero. The angle β is regulated between 0 and 20° in order to reduce and set the extracted power to its maximum value (Bennouk et al., 2016).

The computing of the generator speed and the MPPT strategy is based on the table given by the manufacturer for a 1.5 MW turbine (see Table 1).

The block diagram of the speed reference control is given in Fig. 1.

In order to extract the maximum kinetic power of the wind, the reference of the mechanical speed is regulated according to the variations of the wind speed between the cut-in and cut-out speed, as shown in the wind turbine power curve above (Poitiers, 2003; Gaillard, 2010).

2.3. Machine side converter

The MSC controls the reactive power exchange between the stator and the grid, in addition to controlling the generator torque.

Table 1
Power curve of a wind turbine based on DFIG.

Wind speed (m/s)	Power (KW)
0–3	0
4	150
5	200
6	300
7	500
8	700
9	1000
10	1200
11	1400
12	1500
12–25	1500

The DFIG is connected to the grid, hence the voltage is assumed to be constant. The equations describing the system are presented below (Bui et al., 2015):

$$T_e = \frac{P}{\Omega} = \frac{Pp}{\omega_s} = p(\varphi_{sd} i_{rq} - \varphi_{sq} i_{rd}). \tag{6}$$

The direct and quadrature stator flux components are given by:

$$\varphi_{sd} = \frac{v_{sd} - R_s i_{sd}}{\omega s} \tag{7}$$

$$\varphi_{sq} = \frac{v_{sq} - R_s i_{sq}}{\omega s}$$

i_{rd} and i_{rq} are the direct and quadrature components of the rotor current, v_{sd} and v_{sq} are the direct and quadrature components of the stator voltage.

It is assumed that the stator voltage is oriented along the quadrature axis to simplify the equations:

$$Q_s = -v_{sq} i_{sd}. \tag{8}$$

The new system inputs are respectively the rotor current direct and quadrature components, and the stator reactive power:

$$\begin{aligned} \frac{di_{rd}}{dt} &= \frac{1}{L_r} v_{rd} - \frac{R_r}{L_r} i_{rd} + \omega_r i_{rq} \left(\frac{L_s L_r - M^2}{L_s L_r} \right) \\ \frac{d\varphi_{rq}}{dt} &= v_{rq} - R_r i_{rd} - \omega_r \varphi_{rq} \\ \frac{di_{rq}}{dt} &= -\frac{1}{L_r} v_{rq} + \left(\frac{M^2}{L_s L_r} - \omega_r \right) i_{rd} - \frac{M\omega_r}{L_s L_r \omega_s} v_{sq} - \frac{Rr}{Lr} i_{rq} \\ \frac{dQ_s}{dt} &= -v_{sq} \frac{di_{sd}}{dt}. \end{aligned} \tag{9}$$

A variables change is made to introduce the Lyapunov function:

$$\begin{aligned} y_1 &= Q_C - Q \\ y_2 &= i_{rdref} - i_{rd} \\ y_3 &= i_{rqref} - i_{rq}. \end{aligned} \tag{10}$$

The Lyapunov function is chosen as follows:

$$V_1 = \frac{1}{2} y_1^2 \tag{11}$$

$$\dot{V}_1 = y_1 \dot{y}_1 = y_1 v_{sq} \left(-\frac{R_s}{L_s} i_{sd} - \frac{L_m}{L_s} \frac{di_{rd}}{dt} + \frac{\omega_s}{L_s} \varphi_{sq} \right).$$

The Lyapunov function derivative is strictly negative, if the quantity in parentheses is equal to 0.

The i_{rdref} is given by the following relation:

$$i_{rdref} = -\frac{R_s}{L_s} i_{sd} - \frac{L_m}{L_s} \frac{di_{rd}}{dt} - \frac{\omega_s}{L_s} \varphi_{sq} + i_{rd}$$

$$\dot{y}_2 = \dot{i}_{rdref} - \dot{i}_{rd} - K y_2 + K y_2$$

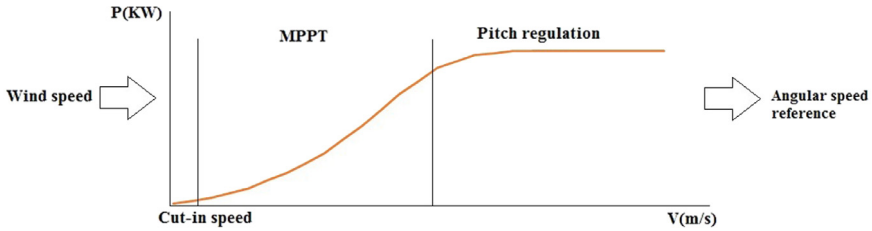

Fig. 1. Wind turbine power curve.

and

$$\dot{y}_3 = \dot{i}_{rqref} - \dot{i}_{rq} - \mathrm{K}y_3 + \mathrm{K}y_3$$

V_2 and V_3 are defined respectively by:

$$\mathrm{V}_2 = \frac{1}{2}\mathrm{y}_2^2 \text{ and } \mathrm{V}_3 = \frac{1}{2}\mathrm{y}_3^2. \tag{12}$$

The V_4 Lyapunov function is defined by:

$$\mathrm{V}_4 = \frac{1}{2}\left(\mathrm{y}_2^2 + \mathrm{y}_3^2 + \mathrm{y}_3^2\right) \tag{13}$$
$$\dot{V}4 = -K\mathrm{y}_2^2 - K\mathrm{y}_2^2 - K\mathrm{y}_3^2 + \mathrm{y}_2\left(\dot{i}_{rdref} - \dot{i}_{rd} + K\mathrm{y}_2\right) + \mathrm{y}_3(\dot{i}_{rdref} - \dot{i}_{rd} + K\mathrm{y}_2).$$

To fulfill the Lyapunov conditions:

$$A_1 = \mathrm{y}_2\left(\dot{i}_{rdref} - \dot{i}_{rd} + K\mathrm{y}_2\right) = 0 \tag{14}$$

and

$$A_2 = \mathrm{y}_3(\dot{i}_{rdref} - \dot{i}_{rd} + K\mathrm{y}_2) = 0.$$

Below are the direct and quadrature rotor voltages:

$$v_{rd} = -K\mathrm{L}_r\mathrm{y}_2 - \mathrm{R}_r i_{rd} + \omega_r\left(LsLr - \frac{M^2}{LsLr}\right) i_{rq} \tag{15}$$
$$v_{rq} = -K\mathrm{L}_r\mathrm{y}_3 + \left(\frac{M^2\omega_r}{\mathrm{L}_s\omega_s} - Lr\omega_r\right) i_{rd} + \frac{M\omega r}{\mathrm{L}_s\omega_s} v_{sq} + \mathrm{R}_r i_{rq}.$$

2.4. Grid-side converter control

The main task of the GSC is the frequency and reactive power regulation. The interconnection to the grid requires that the generator must operate in a frequency between 47 and 52 Hz, and an unbalance not exceeding 2% in the nominal voltage (Mitra and Chatterjee, 0000).

The equations of the system are defined as below (Licari, 2013; Bennouk et al., 2016):

$$U_d = -L\frac{di_{rd}}{dt} - Ri_{rd} + \omega Lirq + v_q \tag{16}$$
$$U_q = -L\frac{di_{rq}}{dt} - Ri_{rq} - \omega Li_{rd} + v_q$$
$$C\frac{d}{dt}v_{dc} = i_{dc} = i_L - i_{rd}$$

U_d, U_q are direct and quadrature components of the converter voltage. v_d and v_q are direct and quadrature components of the transmission grid voltage.

A variables change is made to introduce the Lyapunov function (Muyeen et al., 2010):

$$y_1 = v_{dcc} - v_{dc} \tag{17}$$
$$y_2 = i_{rdc} - v_{dc}$$
$$y_3 = i_{rqc} - i_{rq}.$$

We introduce the Lyapunov function as follows:

$$\mathrm{V}_1 = \frac{1}{2}y_1^2 \tag{18}$$
$$\dot{\mathrm{V}}_1 = y_1\dot{y}_1 = y_1\left(-\frac{dvdc}{dt}\right) = y_1\left(-\frac{1}{C}\left(i_L - i_{rd}\right)\right).$$

The derivative of the Lyapunov function is strictly negative if the i_{rd} reference is set to:

$$i_{rdref} = \mathrm{C}(\mathrm{i}_L + y_1). \tag{19}$$

We then deduce the direct and quadrature voltage components at the GSC:

$$\dot{\mathrm{V}}_2 = y_2\dot{y}_2 = y_2\left(-\frac{dird}{dt}\right) = y_2\left(\frac{Ud}{L} + \frac{R}{L}i_{rd} - \omega i_{rq} - vd\right). \tag{20}$$

To fulfill the Lyapunov conditions, the direct component of the voltage at the DC side is given by:

$$\mathrm{U}_d = -\mathrm{R}i_{rd} + \mathrm{L}\omega irq + \frac{1}{\mathrm{L}}vd - y_2. \tag{21}$$

And:

$$\dot{\mathrm{V}}_3 = y_3\dot{y}_3 = y_3\left(-\frac{dirq}{dt}\right) \tag{22}$$
$$\mathrm{U}_q = -\mathrm{R}i_{rq} + \mathrm{L}\omega i_{rd} + \frac{1}{\mathrm{L}}vq - y_3.$$

2.5. Simulation and results

In this section, the control strategy results are presented with respect to a wind speed with Gaussian noise of zero mean. The stability of the system is analyzed by the verification of the operating parameters at the injection point.

We present in Figs. 2 and 3 the power coefficient and the wind speed graphs including white noise.

The power coefficient reflects very good performances despite the speed variation including white noise. The extracted power is always kept to its maximum thanks to the MPPT strategy based on the continuous calculation of the optimal generator speed as a function of the wind speed.

The turbine speed is shown in Fig. 4. We examine its convergence to the speed reference calculated according to the wind speed and the active power (see Fig. 5).

The turbine speed follows perfectly the wind speed profile; this makes it possible to keep an extracted power permanently equal to the maximum power. This can be seen from the active power profile which changes according to the variation of the wind speed.

The stability of the adopted control strategy can be illustrated by checking the grid parameters, namely the frequency, the HDR, the voltage at the injection point and the active and reactive power profiles. We present various parameters in Figs. 6–8.

From the simulation, we observe that active power profile follows the wind speed variation, while the voltage at the injection point has a stable and balanced profile. The HDR remains below the threshold fixed at 5% in the transmission grid.

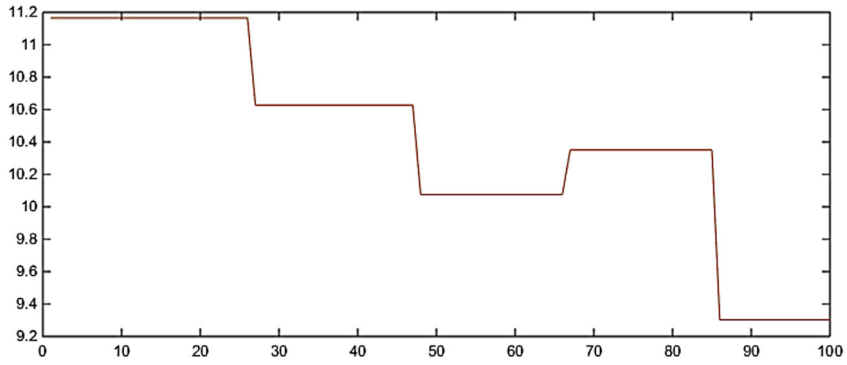

Fig. 2. Wind speed (m/s).

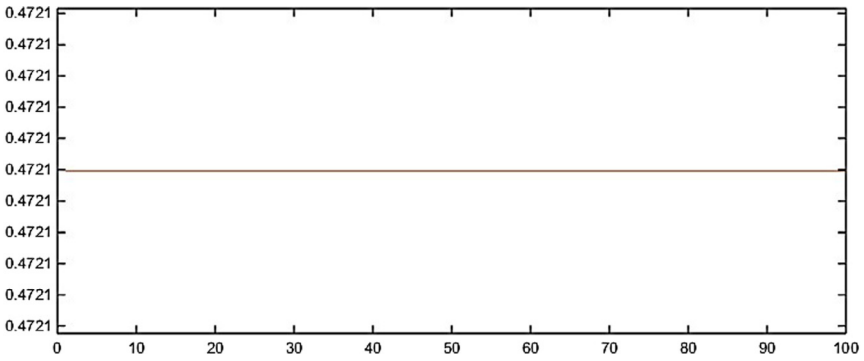

Fig. 3. Power coefficient.

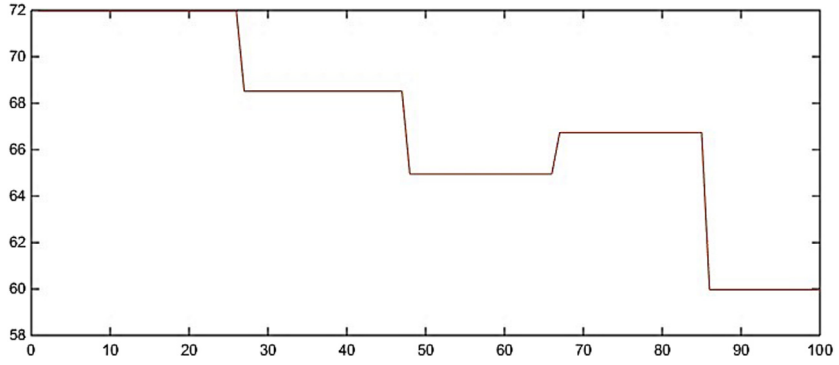

Fig. 4. Turbine speed (rad/s).

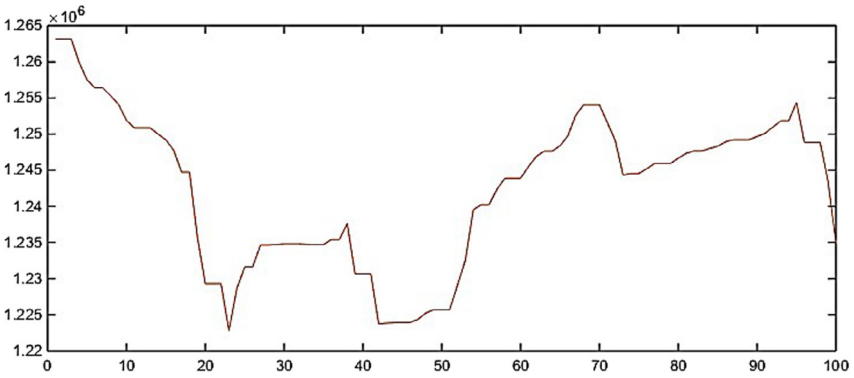

Fig. 5. Active power at injection point (W).

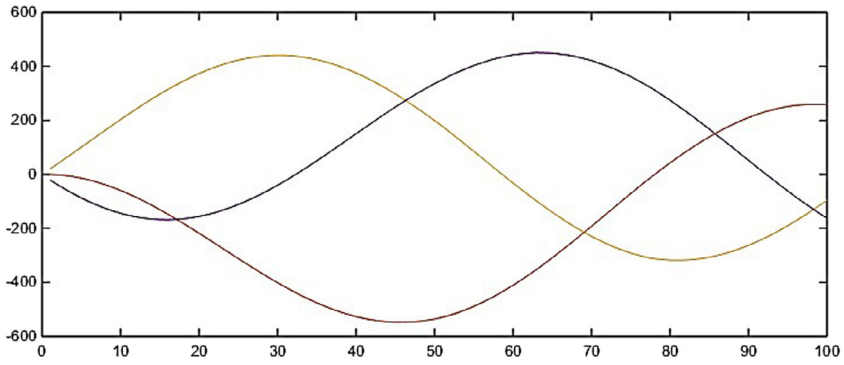

Fig. 6. Currents profile (A).

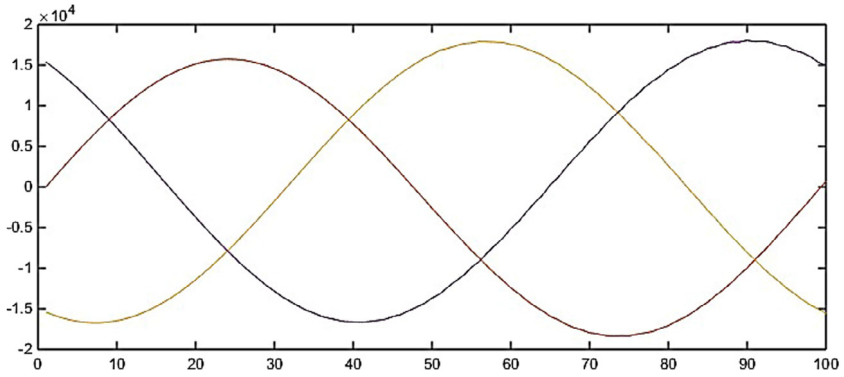

Fig. 7. Voltages profiles (V).

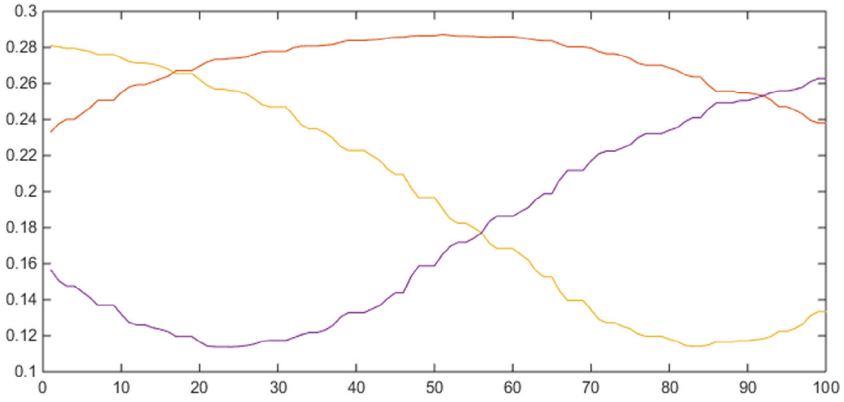

Fig. 8. Voltage HDR (%).

3. Modeling and simulation of an hybrid system

This section presents a hybrid production, composed of two wind turbines connected to the grid. The stability of the system is evaluated by the creation of an electrical fault at the connection point (Bisoyi et al., 0000; Jadhav and Roy, 0000). The control strategies used in our study are similar to those presented in Sections 2.3 and 2.4.

A common method is the parameterization and modeling of transmission lines with passive components. The passive components used in this modeling are resistors, capacitors and inductors. The quantity of these parameters depends mainly on the conductors used in the lines. The lines themselves will have certain characteristics such as longitudinal resistance and reactance, in addition to transversal parameters. There exists also a coupling inductance between lines (Craciu, 2010; Ackermann, 2005).

3.1. Simulation scheme and parameters

In this section, the simulations and results are presented with respect to a wind speed with Gaussian noise of zero mean. The stability of the system is analyzed by the verification of the operating parameters at the injection point. The plant is based on two wind turbines, driven by a DIFG and PMSM and connected to the grid (Fig. 9).

We present in Fig. 10 the results of the simulations for a variable wind speed and a single phase fault.

The estimation of the wind speed is necessary in order to estimate the reference of the turbine speed. The anemometer is disturbed by the wind distribution, with this estimate, it is possible to reduce the error of this effect and consequently increase the maximum power extracted from the turbine.

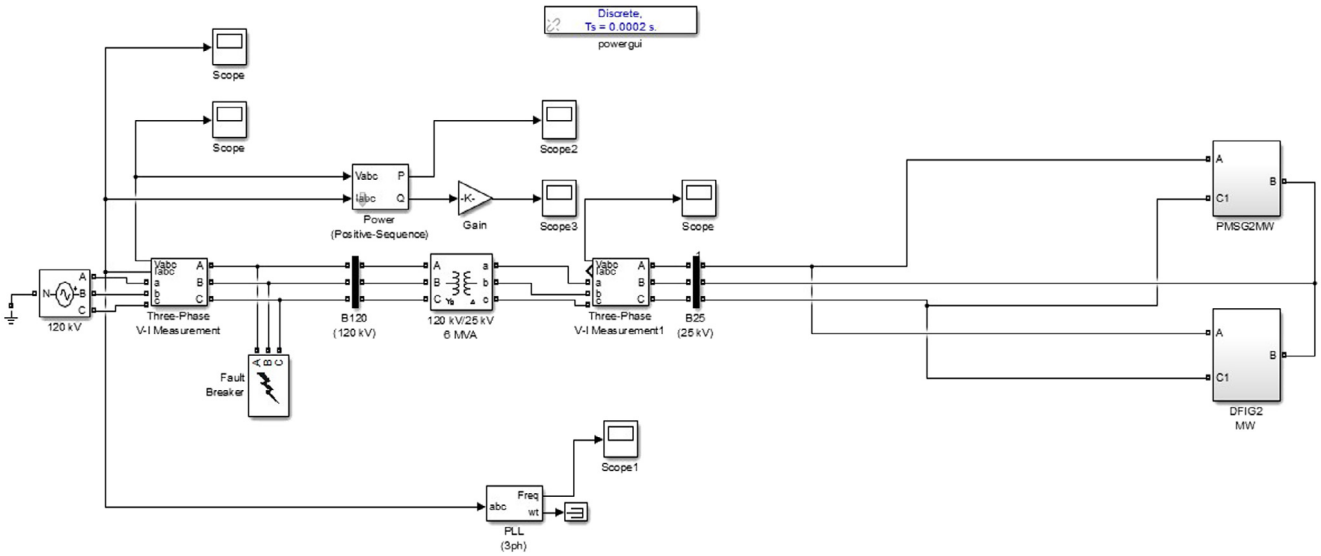

Fig. 9. Hybrid production connected to the transmission grid.

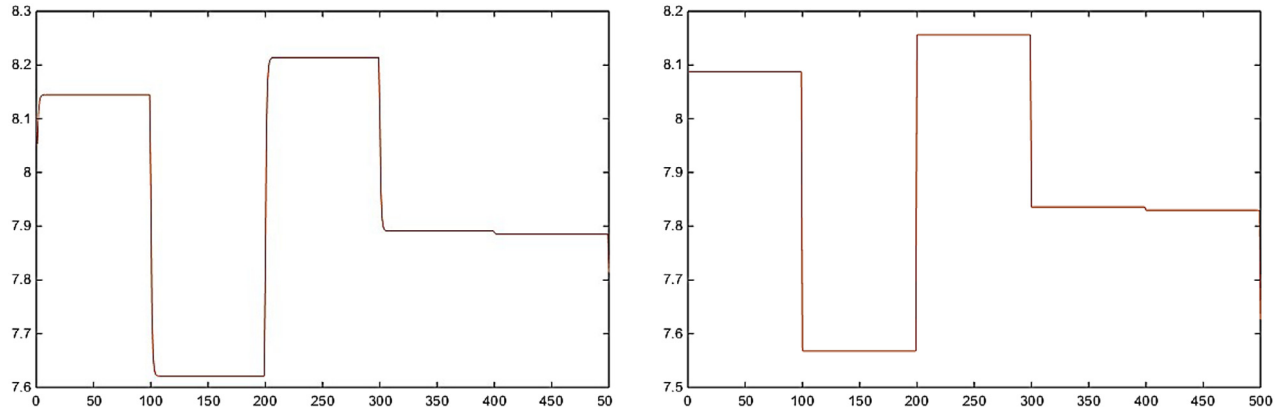

Fig. 10. Wind speed and estimated speeds (m/s).

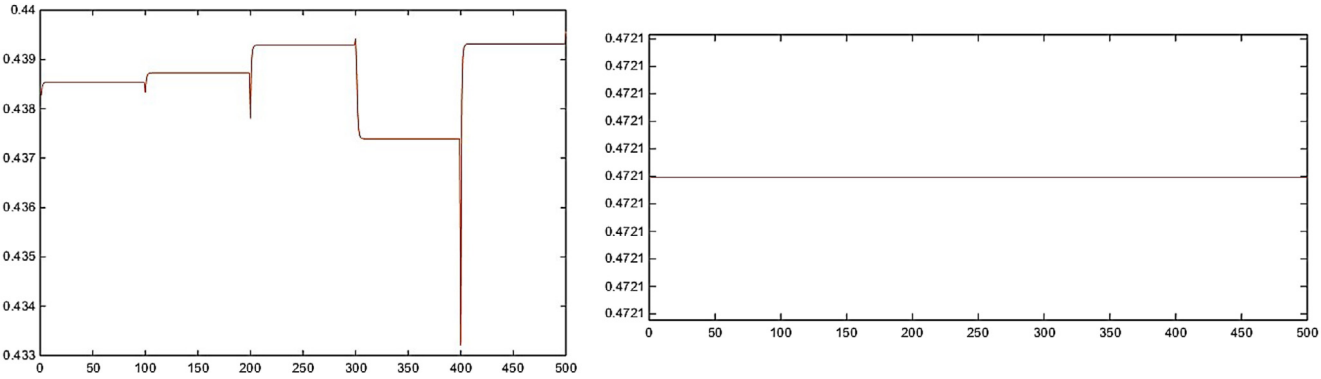

Fig. 11. DFIG and PMSM power coefficients Cps.

To assess the performance of the two turbines, the DFIG and PMSM C_p are presented in Fig. 11.

The error between the estimated and actual speed is close to 0.5%, which validates the Kalman filter as a reliable means of measuring and estimating wind speed. The PMSM power coefficient performances are better than those of the DFIG C_p, in terms of variation and response time (Zou et al., 2013)

To validate the stability of the system, a fault is introduced at the level of the phase-a (Figs. 12 and 13).

The DFIG currents at the injection point show a distortion of *phase-a*, the phase affected by the electrical fault. Yet at the level of the PMSM, we notice that the fault effect was less perceived and the currents resumed their normal balance, after the fault elimination. Here in Figs. 14 and 15 the distortion of the currents.

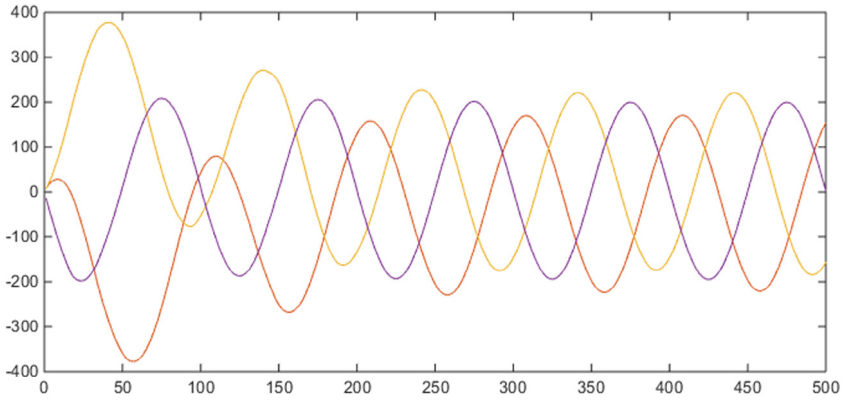

Fig. 12. DFIG currents (A).

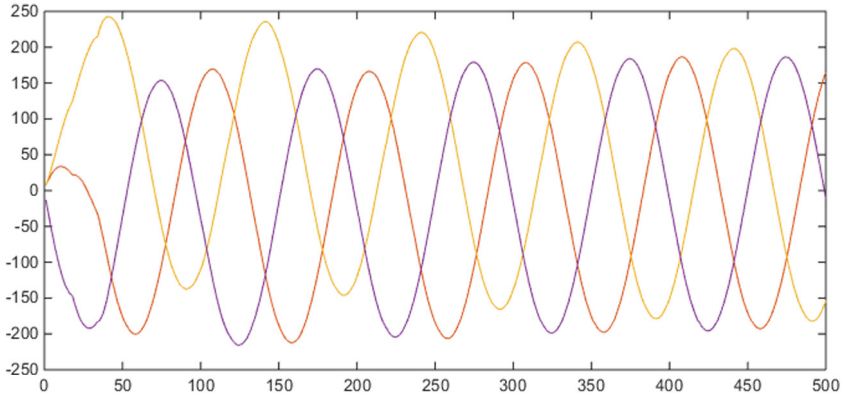

Fig. 13. PMSM currents (A).

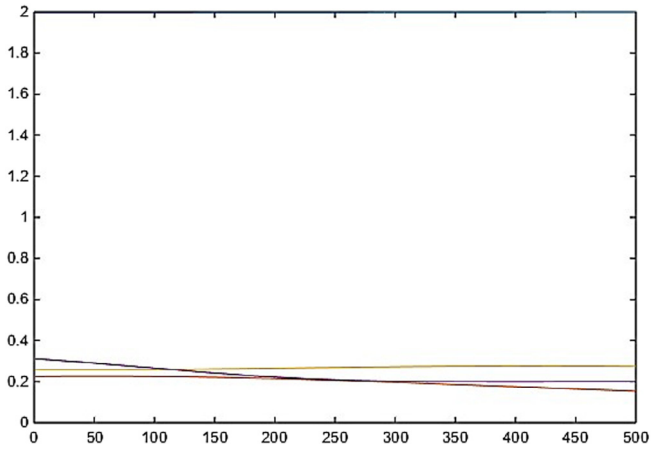

Fig. 14. DFIG currents HDR (%).

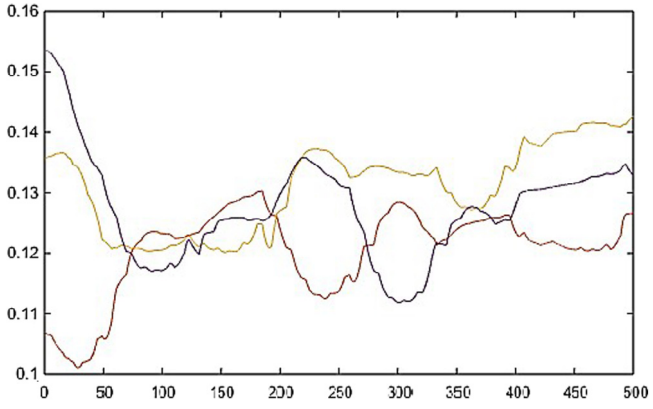

Fig. 15. PMSM currents HDR (%).

From the figures below, we notice that during a single-phase fault in *phase-a*, the two wind turbines present a current unbalance, and a high HDR (0.4%), especially at the DFIG driven wind turbine proximity. A distortion which affects the currents injected into the grid. The PMSM HDR records a low rate, thus respecting the operating parameters standards.

We also evaluate the GSC control performances by analyzing the DFIG and PMSM DC voltages. We present in Fig. 16 the DC bus compensation during the fault created between 0 and 100s.

At the DFIG level, it is noted that during the fault, the voltage reaches three times the reference fixed at 690 V. In order to compensate the crushing of the phase-*a* voltage, the DC voltage fluctuates around its reference. While the PMSM DC bus has shown good performances, since the voltage recover its initial value after fault clearance.

In Fig. 17, the voltage and frequency at the 120KV transmission grid injection point.

The voltage at the injection point is stable without signaling any unbalance exceeding 1%. The frequency also shows a decreasing profile from the time of the fault and remains in the 47–52 Hz margin. The active and reactive powers generated at the 120 KV connection point are presented in Fig. 18.

We notice that the compensation of the PMSM enabled the production of an active power which follows the speed profile.

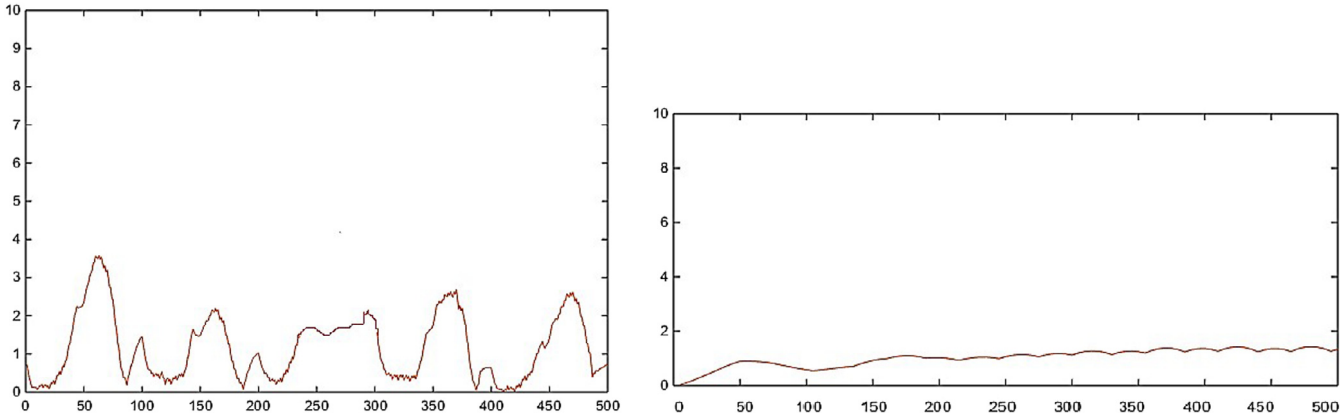

(a) DFIG Udc voltage (pu). (b) PMSM Udc voltage (pu).

Fig. 16. DC bus stability for both DFIG and PMSM (pu).

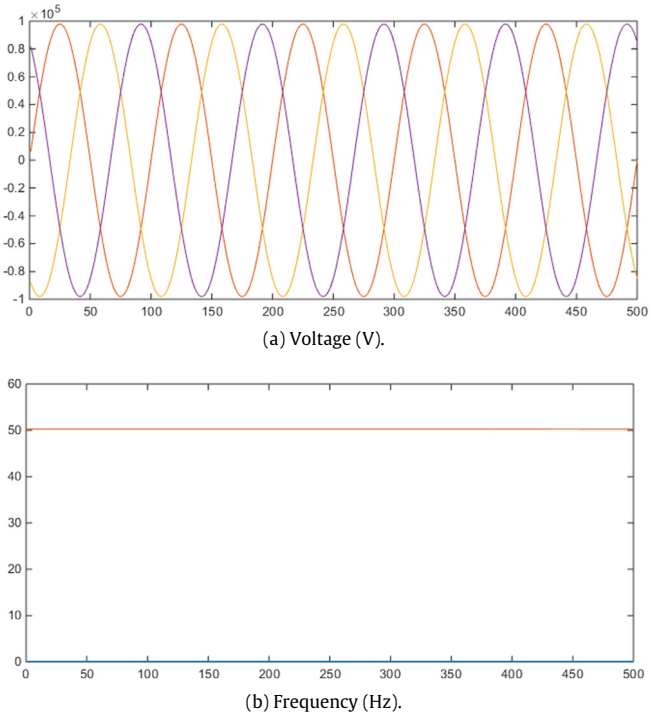

(a) Voltage (V).

(b) Frequency (Hz).

Fig. 17. Transmission line voltage and frequency.

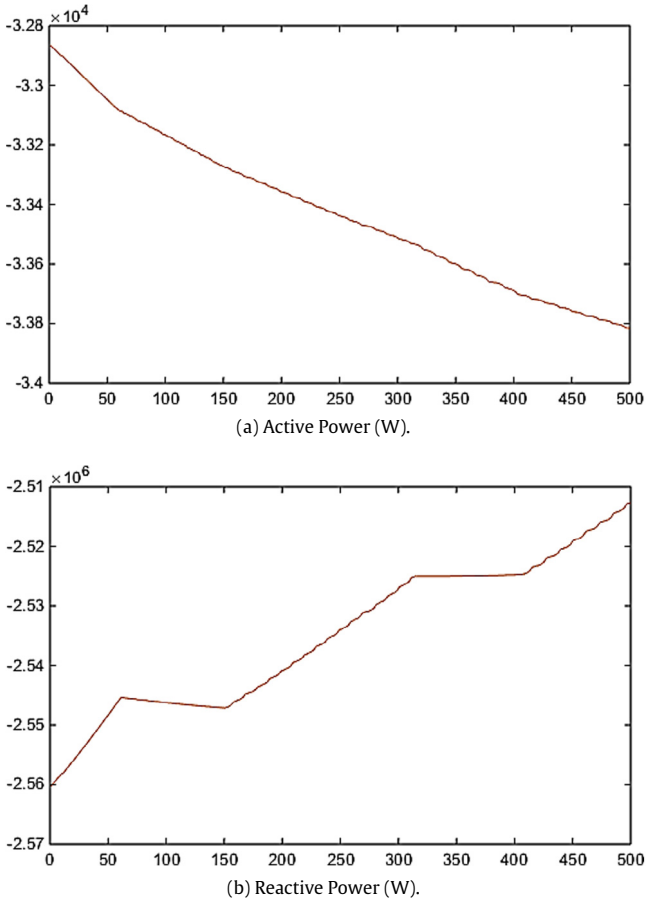

(a) Active Power (W).

(b) Reactive Power (W).

Fig. 18. Active and reactive power at 120kV transmission line.

The reactive power is particularly constant and follows slightly the speed variations.

The PMSM DC voltage profile shows better performances than in the DFIG system. This reflects the stability of the GSC control. The completion of the MPPT was translated by the C_p profile. In the case of PMSM, we notice a dynamic and variable power coefficient, while the DFIG C_p presents a constant profile. We can conclude that the dynamic response of the PMSM wind turbine is faster and more efficient than the DFIG wind turbine.

The adopted GSCs and MSCs controls, in both DFIG and PMSM, have shown good performances in a grid single-phase fault. Lyapunov based control has kept the electromagnetic torque around the reference. The DC bus voltage fluctuates during the fault to compensate the current peak. This is clearly shown in the active power curve, which remains stable during the simulation time.

4. Stability of a wind farm against a single-phase fault in the transmission line

Following a real ground fault in the transmission line, as reported in Fig. 19, the voltage and current profiles during a grid fault in an onshore wind farm located in Morocco. This case study is presented to compare results carried out by simulation with those of a real case, and to see to what extend the simulated systems are similar to a real case study.

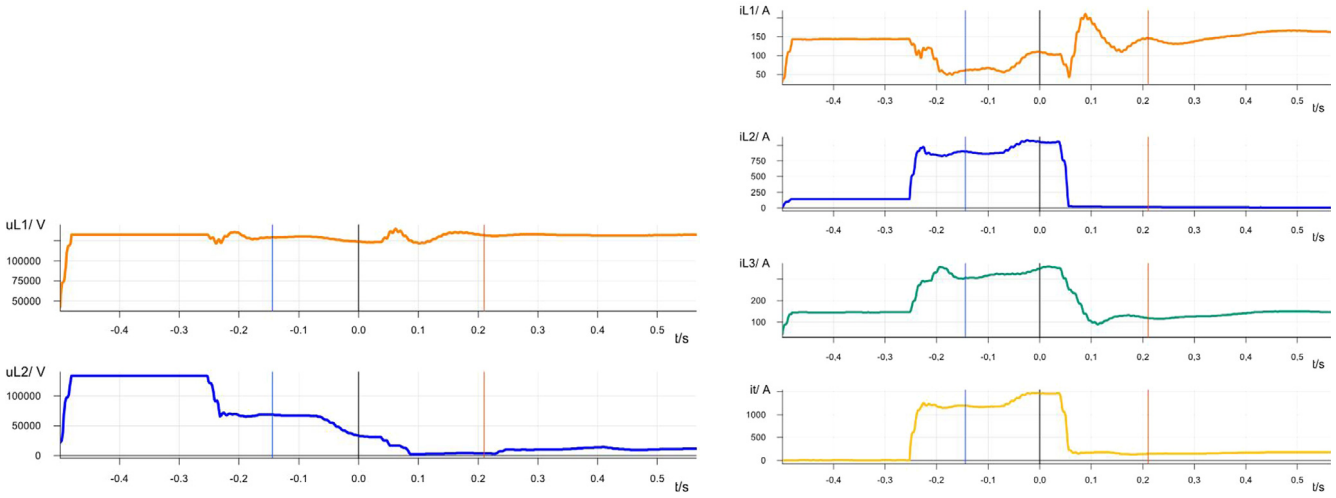

(a) Transmission grid voltage (V).

(b) Transmission grid current (A).

Fig. 19. Voltage and current in transmission grid during phase a fault.

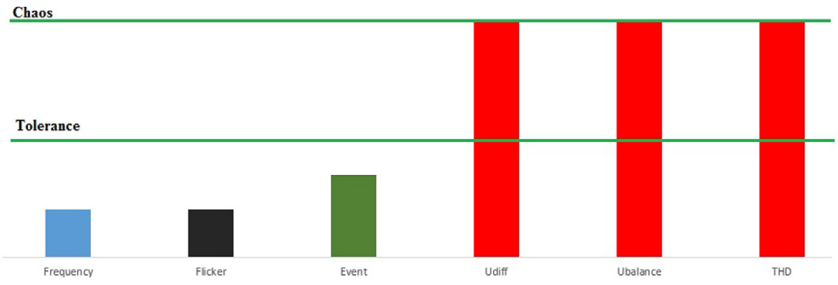

Fig. 20. Energy quality during the fault time.

We notice, from the beginning of the fault, a crushing of the voltage going from 157 KV to 0 in phase 2. The current of the faulted line tends to increase and reached 1200 A in order to compensate this voltage collapse. Hence, the currents unbalance generates a residual earth current.

The different operating parameters are presented, namely HDR, frequency, voltage unbalance and flickers during the fault (Fig. 20).

As presented in the real case, we notice during the grid fault, an overcurrent in the faulted phase, in addition to a distortion in the transmission grid in term of THD and U_{balance}, which reached the chaos threshold. However, the frequency remained in the 47–52 Hz tolerance.

Concerning the simulated case, we conclude that wind turbine driven by PMSM has recorded similar profiles. In fact, we notice also an overcurrent and a distortion in U_{dc} voltage to compensate the overcurrent and keep a stable active power in the coupling point to the transmission grid. As a result of this comparison, we conclude that turbine driven by PMSM presents a normal profile during the simulated fault.

5. Conclusion

This paper presents a hybrid production composed of two turbines based on a DFIG and a PMSM, in order to evaluate their dynamic responses and the stability of the GSC and the MSC for both generators.

In this study, we took as input a real wind speed including a ramp and a Gaussian noise of zero mean, since the anemometer is generally perturbed by the wake effect generated by the blades rotation. We introduced Kalman filter to estimate the value of the speed and then compare it to the actual measurement. The results show a small error between the actual and the estimated speed.

The electrical speed estimation in the simulation was carried out by using a PLL block. The stator and rotor fluxes were calculated on the basis of the currents and according to Eq. (7). The completion of the MPPT as illustrated through the C_p profile for both systems, especially for the PMSM, has a response time and a profile that follows the wind speed variations.

The PMSM shows better performances in terms of stability with respect to a short-circuit fault. The DFIG currents HDR reached 0.45% versus 0.17% for the PMSM, a threshold that clearly affects the current profile in the transmission grid, despite the PMSM compensation. The performances of the PMSM are better in terms of completion of the MPPT strategy. While the DFIG power coefficient presents a dynamic profile that does not comply with the wind speed variations.

References

Ackermann, T., 2005. Wind Power in Power Systems 44. Royal Institute of Technology, Stockholm, Sweden, pp. 1–745.

Bennouk, A., Nejmi, A., Benamou, A., Ramzi, M., 2016. Backstepping and MIMO approachs to control a wind turbine based on DFIG. Int. J. Emerg. Technol. Adv. Eng. 12–17.

Bisoyi, S., Jarial, R.K., Gupta, R.A., 0000. Modeling and control of variable speed wind turbine equipped with PMSG, Int. J. Emerg. Technol. Comput. Appl. Sci. 56–62.

Bui, V., Truong, D., Ho, D., 2015. Dynamic stability improvement of a grid connected wind generators: A case studied. Int. Res. J. Eng. Technol. 2 (08), 1–5.

Craciu, D., 2010. Modélisation des équivalents dynamiques du résea électrique. Institut Polytechniques, Université de Grenoble, pp. 1–175.

Gaillard, A., 2010. Système Éolien Basé Sur Une DFIG: Contribution à L'étude De La Qualité D'énergie Électrique Et La Continuité De Service. Université Nancy, Faculté Des Sciences et Techniques, pp. 1–222.

Jadhav, H.T., Roy, Ranjit, 0000. A comprehensive review on the grid integration of doubly fed induction generator, in: Electrical Power and Energy Systems, Elsevier, pp. 1–11.

Lee, Sung-Hun, Joo, Youngjun, Back, Juhoon, Seo, Jin-Heon, Ick, Choy, 2011. Sliding mode controller for Torque and Pitch control of PMSG wind power systems. J. Power Electron. 11 (3), 342–349.

Li, S., Haskew, T.A., Williams, K.A., Swatloski, R.P., 2012. Control of DFIG wind turbine with direct-current vector control configuration. IEEE 3 (1), 1–11.

Licari, J., 2013. Control of Variable Wind Speed. Institute of Energy, Carddif University, pp. 1–222.

Mitra, A., Chatterjee, D., 0000. Active power control of DFIG-based wind farm for improvement of transient stability of power systems, IEEE, pp. 1–12.

Muyeen, S.M., Takahashi, Rion, Murata, Toshiaki, Tamura, Junji, 2010. A variable speed wind turbine control strategy to meet wind farm grid code requirements. IEEE Trans. 25 (1), 1–10.

Poitiers, F., 2003. Etude et commande de génératrice asynchrone pour l'utilisation en énergie éolienne' 'Ecole polytechnique à l'université de Nantes, Thèse présentée et soutenue le 19 December, pp. 1–168.

Rajendran, S., Jena, D., 2015. Backstepping sliding mode control of a variable speed wind turbine for power optimization. J. Mod. Power Syst. Clean Energy 3 (3), 402–410.

Welch, G., Bish, G., 0000. An Introduction to the Kalman Filters, University of North Carolina at Chapel Hill, pp. 1–81.

Zou, Y., Elbuluk, M., Sozer (Member, IEEE), Y., 2013. Stability analysis of maximum power point tracking (MPPT) method in wind power systems. IEEE Trans. Ind. Appl. 49 (3), 1129–1136.